# Nano-Particle Doped Polymers to Improve Contact Lenses Optical Quality

Lina M. Shaker[1*], Ali H. Al-Hamdani[1] and Ahmed A. Al-Amiery[2]

*[1]Laser and Optoelectronics Engineering Department, University of Technology, Baghdad, Iraq.*
*[3]Energy and Renewable Energy Technology Center, University of Technology, Baghdad 10001, Iraq.*

**ABSTRACT**

*Polymer-based nanocomposites exhibit different optical virtues such as high refractive index (RI), Abbe number ($v_d$) and visible light transmittance (T %) above 90%. These hybrid materials attract more interest in optoelectronic applications such in the ophthalmic optics. The aim of this work is to study the impact of contact lenses doped with aluminum nanoparticles on aberrated human eye. ZEMAX mainstream optical design software was used for eye modeling based on Liou & Brennan eye model and then the BHESP/PA/AL contact lens was applied. Ocular performance was evaluated by modulation transfer function (MTF), spot diagram root mean square (RMS) and the geometric encircled energy (EE) metrics. The used criteria show that the best visual performance is obtained when BHESP/PA/AL-CL is used (P < 0.0001) because it reduced the generated monochromatic and polychromatic aberrations inside the eye. The required balance between the refractive index and abbe number of the chosen polymer affect the transparency, transmittance and refractive errors correction.*

**Keywords:** Nano-Doped Polymer, High Refractive Index, Modulation Transfer Function, Image Simulation.

## 1. INTRODUCTION

Contact lenses (CLs) materials amelioration is now evolving rapidly with biomaterial evolution. Typically, available CLs are based on silicone-hydrogel or polymers, with additional manufacturing techniques employed to produce transparent, colorless, lightweight and impact-resistant lenses. The CLs made for vision correction, therapeutic (drug delivery CLs) [1] to cosmetic appearance purposes required polymers characterized by water and oxygen ($O_2$) permeability, flexibility, high refractive index (RI), high Abbe number ($v_d$) and over 90% transparency at visible light [2,3].

Despite having many pros, the available CLs suffer from various cons such as high oxygen ($O_2$) permeability of Rigid Gas Permeable (RGP) CLs even though they are expensive and require hydrophilic monomers. Modern RGP CLs are more flexible than the hard PMMA CLs due to the integration with low modulus components. RGP lenses have reduced the molar fraction or moved away from hard PMMA polymer content. Nevertheless, they still account for 14% of the CLs in the United States [4] due to their efficiency in reducing corneal aberrations [5]. On the contrary, hydrogel CLs (including soft lenses) are biocompatible [6,7] and inexpensive with enhanced mechanical properties [8,9] but allow a low $O_2$ percentage to transmit to the cornea. One of the characteristics of the silicone hydrogel CLs is durable comfort due to their excellent $O_2$ permeability but they are expensive and need more hydrophilic comonomers to improve

---
*\*Corresponding Author: linamohmmed91@gmail.com*

their water transmission. Another investigation was on PVA modifications as CLs materials. Although Poly(vinyl alcohol) (PVA) CLs [10] exhibit low $O_2$ permeability and fixed water content, they have an improved physical and optical properties, with a transparency of 90% to visible light [11].

Nanocomposites polymers have attracted significant attention in optical applications because of their enhanced optical performance. Recently, nanoparticles (NPs) such as $TiO_2$ [12,13], ZnO [14], ZnS [14,15], $ZrO_2$ [16,17] and so forth have been exploited to obtain high refractive index nanoparticle-polymer composite. These nanocomposites used in the fabrication of optical and biomedical devices such as CLs [18,19]. Among various substitutes, sulfur atom has high atomic refraction, this property makes it an effective candidate in optoelectronic applications [20,21]. Alumina NPs ($Al_2O_3$) also have been employed to further increase the sample RI as well as $\nu_d$ by Bin Cai and his colleagues [22]. They obtained an improved dispersion sulfonyl group triol 1,3-bis(2-hydroxyethylsulfonyl)-2-proponal/phthalic acid (BHESP/PA) of RI = 1.57 and $\nu_d$ = 43.9. Then, they prepared a high-performance optical polymer BHESP/PA/Al from hybridization of synthesized BHESP/PA with well-dispersed alumina NP to increase both RI and $\nu_d$ of the sulfonyl polymer [22]. Inorganic aluminum dioxide NPs has 1.768 RI and very low dispersion of 70 $\nu_d$, used to raise the RI of the based polymer to 1.63 and $\nu_d$ to 53. For transmittance calculations, 20 nm of $Al_2O_3$ was compared with the same size of zirconia NP, the nanocomposite fabricated with alumina maintains 90% transparency in the visible light region.
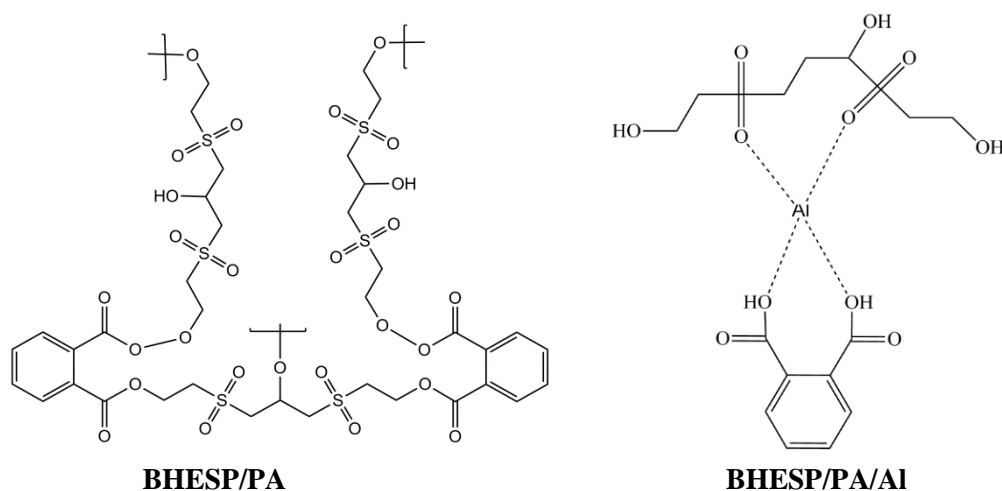


**BHESP/PA**                    **BHESP/PA/Al**

**Figure 1.** Chemical Structure of BHESP/PA polymer and the doped optical polymer with Al NP.

## 1.1 Analysis Criteria

### 1.1.1 Modulation Transfer Function (MTF)

The Modulation Transfer Function (MTF) considers the contrast degradation that occurs in sinusoidal patterns of spatial frequency or the ratio of image contrast to object contrast at all spatial frequencies. Spatial frequency measures the capabilities of the human visual system. The contrast (modulation) of a sinusoidal pattern is defined as [23]:

$$\mathbf{MTF} = \frac{\mathbf{I_{Max}} - \mathbf{I_{Min}}}{\mathbf{I_{Max}} + \mathbf{I_{Min}}} \tag{1}$$

*where* $I_{max}$ is the irradiance of the peak of the sinusoid and $I_{min}$ is the irradiance of the trough of the sinusoid. At a certain value of spatial frequency, the MTF will be zero, this spatial frequency value is called the cutoff frequency ($\nu_{cut\ off}$) and it is given by [24]:

$$V_{cut\ off} = \frac{1}{\lambda(F/\#)} \tag{2}$$

Cut off frequency in equation (2) is measured in Cycles/mm at a specific wavelength ($\lambda$) on the retina. F/# or F/number of an optical system that refers to the ratio of lens focal length (F) to the pupil diameter (PD). For imaging system (human eye), the standard conversion of spatial frequency from Cycles/mm unit to Cycles/degree is [24]:

$$100\frac{Cycles}{mm} = 30\frac{Cycles}{degree} \tag{3}$$

### 1.1.2 Root Mean Square (RMS)

Spot diagram is a method for visualizing the aberration effect on image quality and hence lens resolution. Another measure of quality that realizes on the spot diagram is the RMS spot radius [25], RMS; RMS belong to the root mean square of the spot in the image plane. The RMS spot radius is defined as [26]:

$$r_{RMS} = \sqrt{\frac{\sum_{i=0}^{N} r_i^2}{N}} \tag{4}$$

Where $N$ represents the total number of rays traced, $r_i$ refers to the distance between two points.

### 1.1.3 Encircled Energy (EE)

Encircled Energy (EE) refers to a measure of accumulated energy in an optical image. EE is indicated in the following formula [27]:

$$EE(z) = \int_0^{2\pi} \int_0^1 PSF(r)rdrd\varphi \tag{5}$$

$$PSF = \int_{-\infty}^{\infty} f(x)exp - \{i2\pi\upsilon x\}\,dx \tag{6}$$

Where PSF represents the point spread function which is the Fourier Transformation of the pupil function $f(x)$ and it is a measure of shape and size of the point source image.

In this paper, the ZEMAX optical design program used to evaluate and model the optics of BHESP/PA/AL-CL based on the commonly used eye model Liou & Brennan eye (L&B). MTF, EE and the spot diagram enabled image performance analysis when fitted on the human eye.

## 2. OPTICAL MODELING

An optical design program ZEMAX was used for computer eye modeling and simulation based on the L&B eye model (healthy eye) and BHESP/PA/Al CL. All ray-tracing simulations were performed at two conditions of monochromatic light at 555 nm with weight of 1 and the *photopic (Bright)* spectrum of 470, 510, 555, 610 and 650 nm wavelengths with weights of 0.091, 0.503, 1, 0.503 and 0.107, respectively. L&B model was chosen in this study because it was obtained experimentally from the human eye [28].

Optical parameters of the eye (see Table 1) and the mentioned CL (see Table 2) are entered into ZEMAX software. The two surfaces of the cornea (anterior and posterior cornea) were selected

as aspherical surfaces (named standard surface in ZEMAX). The standard surface requires two specific parameters: radius and conic constant. The pupil aperture surface was selected as stop aperture and decentered by 0.5 mm nasally with respect to the visual axis [29,30]. The crystalline lens was represented by two homogeneous gradient index shells whose RI is described by:

$$n = n_0 + n_{r2}r^2 + n_{r4}r^4 + n_{r6}r^6 + n_{z1}z + n_{z2}z^2 + n_{z3}z^3 \tag{7}$$

$$r^2 = x^2 + y^2 \tag{8}$$

The vitreous body of the eye and finally the imaging surface of the retina. The standard surface position is centered on the optical axis and its vertex located at the z-axis. The "sag" of the standard surface is given by [25]:

$$z = \frac{cr^2}{1+\sqrt{1-(1+Kc^2r^2)}} \tag{9}$$

Where c is the curvature (the reciprocal of the radius), r is the radial coordinate in the lens unit and K is the conic constant. The extended polynomial surface was used to insert the front surface of the applied CL. The sag of this aspherical surface is given by the expression:

$$z = \frac{cr^2}{1+\sqrt{1-(1+K)c^2r^2}} + \sum_{i=1}^{N} A_i E_i(x, y) \tag{10}$$

Where $N$ refers to the number of polynomial coefficients in the series, $A_i$ is the coefficient on $i^{th}$ extended polynomial term.

**Table 1** Input parameters of the L&B eye model in ZEMAX software

| Surface | Radius [mm] | Thickness [mm] | RI | $\nu_d$ | Conic | PD [mm] |
|---------|-------------|----------------|------|---------|-------|---------|
| Cornea (anterior cornea) | 7.77 | 0.55 | 1.376 | 50.23 | -0.18 | 10 |
| Aqueous (posterior cornea) | 6.40 | 3.16 | 1.336 | 50.23 | -0.6 | 10 |
| Pupil | Infinity | 0 | 1.34 | 50.23 | 0 | 4 |
| Lens-Front surface | 12.40 | 1.59 | - | - | 0 | 10 |
| Lens-Back surface | Infinity | 2.43 | - | - | 0 | 10 |
| Vitreous humor | -8.1 | 16.24 | 1.336 | 50.23 | 0.96 | 10 |
| Retina | -12 | - | - | - | 0 | 10 |

**Table 2** Construction data of polymeric BHESP/PA/Al CL, radius and thickness are measured in mm

| Material | CL Front Radius | CL Back Radius | CL Front Thickness | CL Back Thickness | RI | $v_d$ |
|---|---|---|---|---|---|---|
| BHESP/PA/Al | 7.748 | 7.8 | 0.1 | 7.8 | 1.63 | 53 |
| Conic = 0.035, PD = 4 mm and F.O.V. = 5 degrees | | | | | | |

## 3. RESULTS

For particular input specifications, the contrast transmission produced by aberrated eye and treated eye with CL was observed from MTF metric and its graphical data as the focusing criterion. Spot diagram RMS and geometric EE (as a function of radius from centroid) were obtained at the same off-axis field and pupil Semi-Diameter for the retinal image quality evaluation.

### 3.1 MTF Response

Maximum MTF values were set at 30 Cycles/mm as the optimum contrast area. 5-degree off-axis tangential component of MTF measured at 555 nm monochromatic light and polychromatic light ranging from 470-650 nm for both models. MTF curves refer to the retinal image contrast, illustrated in Figure (2). The blue dashed line represents the L&B eye model when the system operated at white light which exhibits an averaged MTF ± Standard Deviation (SD) of 0.8 ± 0.06. It diminished quickly than that produced by the monochromatic light (0.9 ± 0.05). This is due to the exposure of the spherical and chromatic aberrations when the pupil diameter (PD) is enlarged to 4 mm from its optimal size. The generated spherical aberration in L&B model (blue solid line) was the reason of MTF degradation, which means focusing the light in a large spot on the retina caused the photoreceptors to receive a low amount of light. The best vision improvement as a function of frequency response was achieved when applying the contact lens, especially in L&B model when a monochromatic light was applied. In this case, BHESP/PA/Al CL eliminated the generated spherical aberration by focusing the incoming rays at the same point on the retina which is clear from the solid red line of MTF, where the MTF value approached from 1. Thus, this aberrated eye is corrected with aspherical low dispersion BHESP/PA/Al CL. MTF response of the corrected eye raised for both light sources. The highest MTF curve represented by the red solid line, realized by 555 nm (0.92 ± 0.04) of the inserted CL. A slight decrease in image contrast was obtained when the CL is operated at white light of mean MTF = 0.9 ± 0.05. Typically, human eye cut-off frequency exceeds the ability to perceive the higher frequencies due to the generated aberrations and the scatter resulting in ocular media. Cut-off frequencies of MTF curves for all cases are given in Table 3 in Cycle/mm units and its conversion to the Cycle/degree units based on Equation 3. Image simulation illustrated in Figure (3) explains the impact of doped lenses in both cases at 555 nm and polychromatic light on image quality. Less Image contrast obtained as the spatial frequency increases in addition to the generated off-axis and on-axis aberrations obtained by the free-lenses eye (Figures 3.a. and 3.c) which improved after the CL was applied (Figures 3.b. and 3.d.).

**Table 3** Cut off frequency conversion of a human eye response

| Light source | Model | $v_{cutoff}$ (cycles/mm) | $v_{cutoff}$ (cycles/degree) |
|---|---|---|---|
| 555 nm | L&B | 495 | 149 |
| | BHESP/PA/Al CL | 495 | 149 |
| 470-650 nm | L&B | 585 | 176 |
| | BHESP/PA/Al CL | 565 | 170 |
| F# = 3.7, F = 16.6 mm, PD = 4 mm, F.O.V. = 5 degrees | | | |
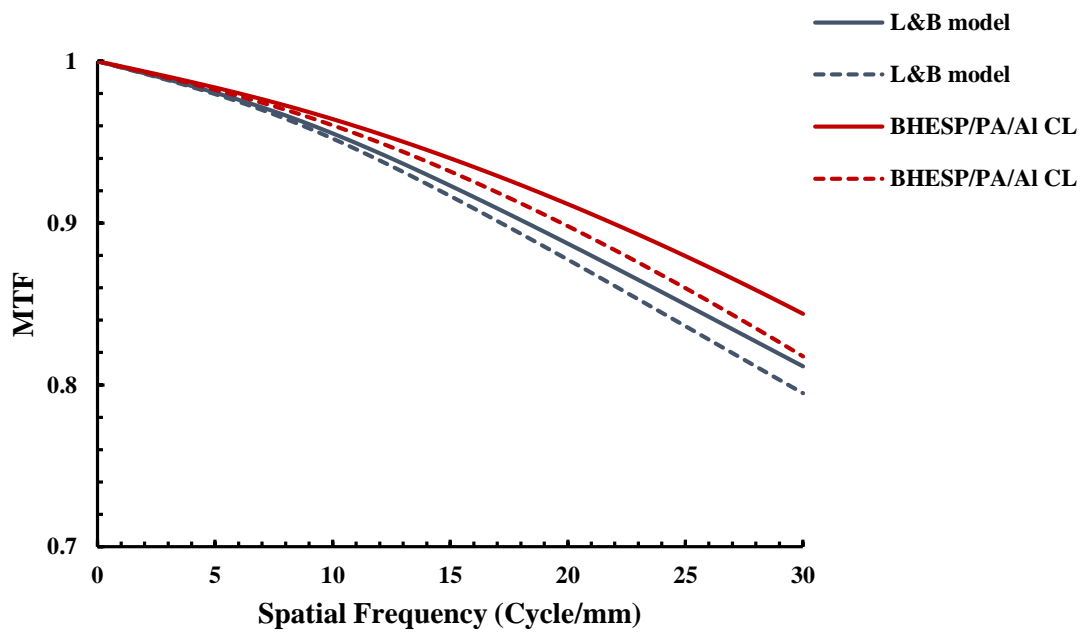


**Figure 2.** MTF evaluation at 555 nm wavelength represented by the blue and red solid curves for the aberrated eye and treated eye with Al-doped CL, respectively. MTF at polychromatic light range 470-650 nm represented by blue and red dashed lines for both aberrated eye and treated eye with Al-doped CL, respectively.

**Figure 3.** Image simulation of a. aberrated model at 555 nm. b. Al-doped CL at 555 nm. c. aberrated model at (470-650 nm). d. Al-doped CL at (470-650 nm).

## 3.2 Geometric Encircled Energy and Spot Diagram

When the object moving away from the eye, the pupil size enlarges and a wider beam of light enters to cause deformation in the image focused on the retina. Two metrics (EE and RMS) were used to calculate the spot radius difference and to identify which kind of aberration causes the deformation. Geometric EE plot is given as a fraction of enclosed energy (%) as a function of radius from the spot center. RMS of the spot diagram is another function used to show if the inserted doped CL minimize the spot radius and overcome the generated aberration inside the eye. The RMS value is measured in μm. RMS diagram gives an indication of the amount of aberration and its kind. Unlike the MTF curves, the highest amount of aberrations appear when the spot size is large (highest values of RMS), indicating that little amount of energy is accumulated on the retina.

In Figure 4, the slope of each curve represents the amount of rays in spot (x-axis) diameter. High slope means a small spot size which represents the best image performance. At 555 nm light source, fractional EE and spot diagram of both aberrated and treated eye are shown in Figure (4.a.). High slope achieved by the red line represents the doped-CL fractional energy. The blue curve belongs to energy accumulated on the retina of the aberrated eye. At 50%, the maximum radius difference between the two models is slightly less than 4 microns. Energy response of doped CL is higher than the free lenses eye indicating the energy accumulates in a small spot (low value of RMS) on the retina. This demonstrated by the spot diagrams in Figure (4.b.). The smaller the RMS, the more accumulated energy on the retinal surface. Spherical aberration (on-axis aberration) presence caused an enlargement in aberrated eyespot size to 7.316 μm. This defect was treated by aluminum-doped aspherical CL. The effect of CL appears in spot minimization to 3.438 μm.
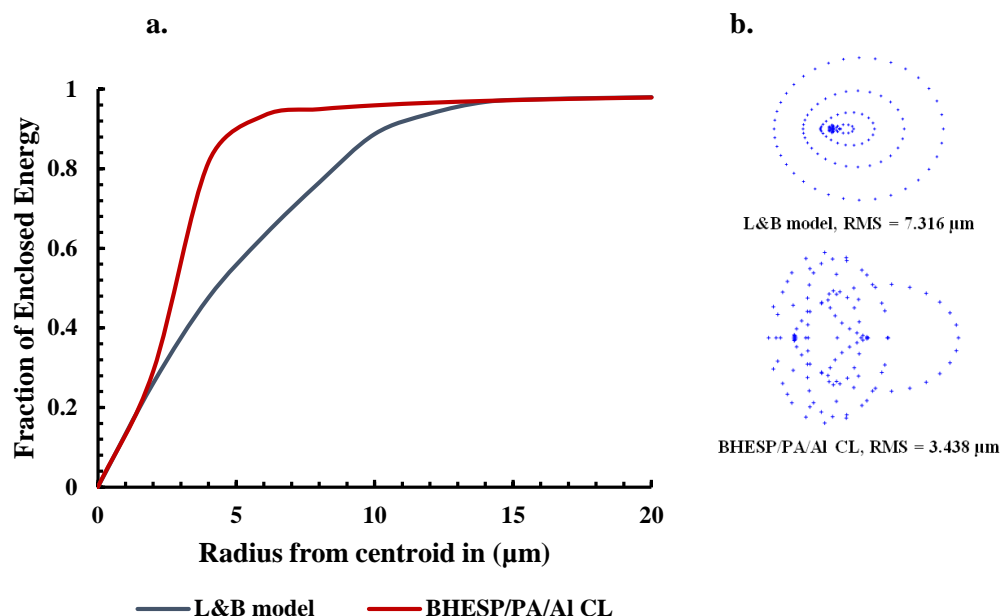
**a.**
**b.**



**Figure 4.** (a) EE of monochromatic light as a function of radius from centroid for aberrated eye (blue solid curve) and corrected eye with Al-doped CL (red solid curve). (b) Spot diagram of monochromatic light the blue dots refer to the 555 nm light effect.

Figure 5.a. shows the accumulated energy on the retina when it is affected by the polychromatic light. The blue dashed line refers to L&B eye which is far from the y-axis to cause a large spot of 7.046 μm RMS as a result of spherical aberration and light dispersion (light rays focused in different focal points); this is called chromatic aberration. The energy fraction at 50% was improved when the CL was applied where the spot RMS minimized to 3.827 μm. In this case, generated chromatic aberration was reduced by the doped lenses because the alumina NPs increases the $v_d$ of the based polymer suggesting dispersion reduction.

Monochromatic light produced small spot size and high accumulated energy than the polychromatic light because divergence of polychromatic light beam increases the spot size. It is clear from Figure (4.b.) and (5.b.) that similar spot shapes were yielded when comparing the effects of 555 nm and white light on the L&B model and the polymeric CL. Differing by the emergence of axial and lateral chromatic aberrations denoted by W020 and W111, respectively in addition to the spherical aberration W040 which optically enhanced by the BHESP/PA/Al CL. While coma and astigmatism, as well as distortion, didn't appear clearly because of the natural small off-axis F.O.V. of human eye.
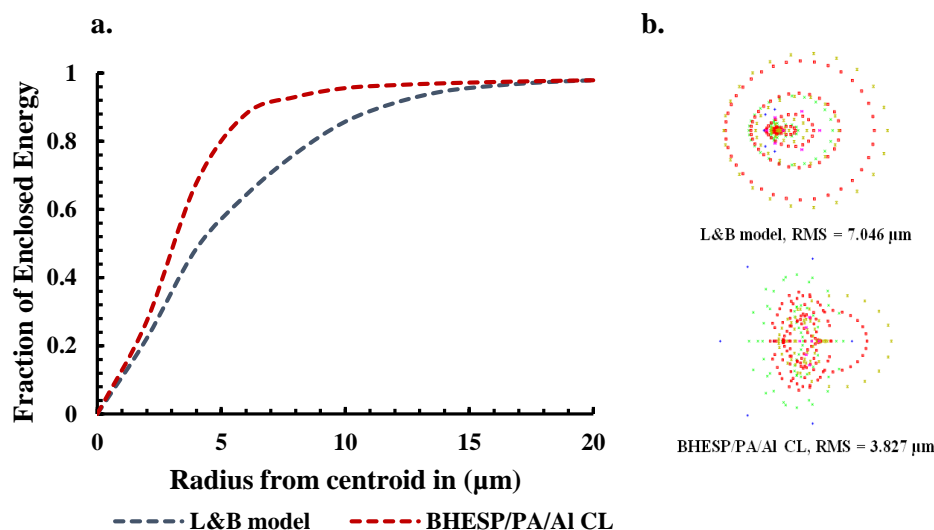
**Figure 5.**(a) EE of polychromatic light as a function of radius from centroid for both aberrated eye (blue dashed curve) and corrected eye with Al-doped CL (red dashed curve). (b) Spot diagram of polychromatic light the blue, green, red, yellow and purple dots represent the effect of 470, 510, 555, 610, 650 nm wavelengths, respectively.

## 4.  CONCLUSION

NP material doped CLs is considered as a promising device to improve the retinal image properties. The obtained results of BHESP/PA/Al CL programming test are encouraging. However, further cytotoxic and mechanical studies on alumina-NP impact are required. The aim of this work was to investigate the effect of Al-doped CLs on image performance when the human eye operates at monochromatic and polychromatic light sources. The present study exhibited a closer MTF response to the diffraction-limited MTF of healthy eye by the use of the mentioned CL. Regardless of cut off frequency value, the highest image contrast was realized at 555 nm. The introduced monochromatic and polychromatic aberrations were minimized. Spherical Aberration (SA) cannot be altered by CL bending since its shape must be fixed to comply with corneal shape. Despite that, the applied aspheric front surface CL minimized the SA level and not eliminated it, by focusing the edge and central rays in a small spot on the retinal surface. This CL made up from Al-doped polymer of high RI and low dispersion, it reduced both of the axial colors defocus and lateral color tilt produced by polychromatic light source.

## REFERENCES

[1]  A. Guzman-aranguez & B. Colligris, "Contact Lenses : Promising Devices for Ocular Drug Delivery," J Ocul Pharmacol Ther. **29**, 2 (2013) 189–199.

[2]  F. A. Maulvi, A. A. Shaikh, D. H. Lakdawala, A. R. Desai, M. M. Pandya, S. S. Singhania, R. J. Vaidya, K. M. Ranch, B. A. Vyas & D. O. Shah, "Design and optimization of a novel implantation technology in contact lenses for the treatment of dry eye syndrome : In vitro and in vivo evaluation," ACTA BIOMATER. **53** (2017) 211–221.

[3]  Q. Zhang, Z. Fang, Y. Cao, H. Du, H. Wu, R. Beuerman, M. B. Chan-park, H. Duan & R. Xu, "High Refractive Index Inorganic – Organic Interpenetrating Polymer Network (IPN) Hydrogel Nanocomposite toward Artificial Cornea Implants," ACS Macro lett. **1** (2012) 876–881.

[4] N. Efron, "Obituary —Rigid contact lenses," Contact Lens Anterior Eye **33** (2010) 245–252.

[5] F. Shokrollahzadeh, H. Hashemi, E. Jafarzadehpur & A. Mirzajani, "ScienceDirect Corneal aberration changes after rigid gas permeable contact lens wear," J Curr Ophthalmol. **20**, (2016) 1–5.

[6] F. J. HOLLY, "Basic aspects of contact lens biocompatibility," Colloids Surf. **10** (1984) 343–350.

[7] T. Goda & K. Ishihara, "Soft contact lens biomaterials from bioinspired phospholipid polymers," Expert Rev. Med. Devices **3**, 2 (2006) 167–174.

[8] C. Maldonado-Codina & N. Efron, "Dynamic wettability of pHEMA-based hydrogel contact lenses," Ophthalmic Physiol. Opt. **26** (2006) 408–418.

[9] E. Seo, S. Kumar, J. Lee, J. Jang, J. H. Park, M. C. Chang, I. Kwon, J. S. Lee & Y. il Huh, "Modified hydrogels based on poly(2-hydroxyethyl methacrylate) (pHEMA) with higher surface wettability and mechanical properties," Macromol. Res **25** (2017) 704–711.

[10] M. Kita, Y. Ogura, Y. Honda, S.-H. Hyon, W.-I. Cha & Y. Ikada, "Evaluation of polyvinyl alcohol hydrogel as a soft contact lens material," Graefe's Arch. Clin. Exp. Ophthalmol **228**, (1990) 533–537.

[11] G. K. Tummala, R. Rojas & A. Mihranyan, "Poly(vinyl alcohol) Hydrogels Reinforced with Nanocellulose for Ophthalmic Applications: General Characteristics and Optical Properties.," J. Phys. Chem. B **120** (2016) 13094–13101.

[12] Z. Cui, C. Guan, J. Guan, B. Yang & J. Shen, "Research on Preparation, Structure and Properties of TiO 2 / Polythiourethane Hybrid Optical Films with High Refractive Index," Macromol. Mater. Eng. **288**, 9 (2003) 717–723.

[13] B. T. Liu & P. S. Li, "Preparation and Characterization of High-Refractive-Index Polymer/Inorganic Hybrid Films Containing TiO2 Nanoparticles Prepared by 4-Aminobenzoic Acid.," Surf. Coat. Technol. **231** (2013) 301–306.

[14] M. M. Demir, K. Koynov, C. Bubeck, I. Park, I. Lieberwirth & G. Wegner, "Optical Properties of Composites of PMMA and Surface-Modified Zincite Nanoparticles," Macromolecules **40** (2007) 1089–1100.

[15] J. Xu, Y. Zhang, W. Zhu & Y. Cui, "Synthesis of Polymeric Nanocomposite Hydrogels Containing the Pendant ZnS Nanoparticles: Approach to Higher Refractive Index Optical Polymeric Nanocomposites," Macromolecules **51**, 7 (2018) 2672–2681.

[16] Y. Xia, C. Zhang, J. X. Wang, D. Wang, X. F. Zeng & J. F. Chen, "Synthesis of Transparent Aqueous ZrO2Nanodispersion with a Controllable Crystalline Phase without Modification for a High-Refractive-Index Nanocomposite Film," Langmuir **34**, 23 (2018) 6806–6813.

[17] Y. Xia, C. Zhang, J. Wang, D. Wang, X. Zeng & J. Chen, "Synthesis of Transparent Aqueous ZrO2 Nanodispersion without Modification for High-Refractive-Index Nanocomposite Film Synthesis of Transparent Aqueous ZrO 2 Nanodispersion with Controllable Crystalline Phase without Modification for High-Refractive-Index," Langmuir **34**, 23 (2018) 6806–6813.

[18] A. H. Al-hamdani, "Design and Performance Analysis of Contact Lens Materials for Chromatic and Polychromatic Aberrations Correction," Eng. Technol. J. **36**, 9 (2018) 1016–1021.

[19] A. H. Al-hamdani & A. H. Halah, "Effect of field of view and iris pupil diameter on the quality of retinal image with allyl carbonate ( CR-39 ) polymer contact lenses Effect of field of view and iris pupil diameter on the quality of retinal image with allyl carbonate ( CR-39 ) polymer co," IOP Conf. Ser. Mater. Sci. Eng. 454 012081 (2018).

[20] R. Okutsu, Y. Suzuki, S. Ando & M. Ueda, "Poly ( thioether sulfone ) with High Refractive Index and High Abbe ' s Number," Macromolecules **41**, 16 (2008) 6165–6168.

[21] M. Maheswara, S. H. Oh, J. J. Ju, S. K. Park, S. Park & J. Y. Do, "High refractive index of transparent acrylate polymers functionalized with alkyl sulfur groups," Polym. J. **42**, 3 (2010) 249–255.

[22] B. Cai, T. Kaino & O. Sugihara, "Sulfonyl-containing polymer and its alumina nanocomposite with high Abbe number and high refractive index," Opt. Mater. Express **5**, 5 (2015) 1210.

[23] E. Hecht, "Optics," 5th ed., England: Pearson Education Limited, (2017) 579.

[24] M. Schaub, J. Schwiegerling, E. C. Fest, A. Symmons & R. H. Shepard, Molded Optics: Design and Manufacture. Taylor and Francis Group, LLC, (2011).

[25] Joseph M. Geary, Glass & the LandScape Lens., (2002).

[26] H. Sun, "Lens design: a practical guide," Taylor & Francis Group, (2017) 103.

[27] J. R. Max, Optical Design Fundamentals for Infrared Systems, 2nd ed. SPIE Press, (2001).

[28] N. A. Brennan & H.-L. Liou, "Anatomically accurate, finite model eye for optical modeling," Opt. Soc. Am. **14**, 8 (1997) 1684–1695.

[29] G. Westheimer, "Image Quality in the Human Eye," Opt. Acta  Int. J. Opt. **17**, 9 (1970) 37–41.

[30] S. Dua, U. R. Acharya & E. Y. K. Ng, Computational Analysis of the Human Eye with Applications. World Scientific, (2011).